nature medicine

STAT3 signaling controls satellite cell expansion and skeletal muscle repair

Matthew Timothy Tierney[1,6], Tufan Aydogdu[2,3,6], David Sala[2], Barbora Malecova[2], Sole Gatto[2], Pier Lorenzo Puri[2,4], Lucia Latella[4,5] & Alessandra Sacco[2]

The progressive loss of muscle regenerative capacity with age or disease results in part from a decline in the number and function of satellite cells, the direct cellular contributors to muscle repair[1–11]. However, little is known about the molecular effectors underlying satellite cell impairment and depletion. Elevated levels of inflammatory cytokines, including interleukin-6 (IL-6), are associated with both age-related and muscle-wasting conditions[12–15]. The levels of STAT3, a downstream effector of IL-6, are also elevated with muscle wasting[16,17], and STAT3 has been implicated in the regulation of self-renewal and stem cell fate in several tissues[18–21]. Here we show that IL-6–activated Stat3 signaling regulates satellite cell behavior, promoting myogenic lineage progression through myogenic differentiation 1 (Myod1) regulation. Conditional ablation of *Stat3* in Pax7-expressing satellite cells resulted in their increased expansion during regeneration, but compromised myogenic differentiation prevented the contribution of these cells to regenerating myofibers. In contrast, transient Stat3 inhibition promoted satellite cell expansion and enhanced tissue repair in both aged and dystrophic muscle. The effects of STAT3 inhibition on cell fate and proliferation were conserved in human myoblasts. The results of this study indicate that pharmacological manipulation of STAT3 activity can be used to counteract the functional exhaustion of satellite cells in pathological conditions, thereby maintaining the endogenous regenerative response and ameliorating muscle-wasting diseases.

Chronic inflammation is a hallmark of several muscle-wasting diseases and impairs the normal regenerative response. IL-6 is among the inflammatory cytokines present during the initial stages of muscle repair and can exert both pro- and anti-regenerative effects[16]. Although sustained, systemic elevation of IL-6 contributes to muscle atrophy[14,22], IL-6 also acts as an essential regulator of satellite cell–mediated hypertrophy[23], underlying its pleiotropic role during skeletal muscle maintenance. We hypothesized that intervening downstream of IL-6 signaling may allow for selective interference with its deleterious outcomes and enhance satellite cell function. The JAK-STAT pathway serves as an intracellular mediator of IL-6 signaling and is evolutionary conserved from flies to mammals[24,25]. Cytokine binding to the IL-6r–Gp130 receptor complex leads to JAK activation and STAT phosphorylation on tyrosine residues, STAT dimerization, nuclear translocation and target gene activation[26,27]. Among the *Stat* genes, *Stat3* has a critical role during development as evidenced by the early embryonic lethality of *Stat3*$^{-/-}$ mice[28]. In skeletal muscle, Stat3 has been shown to regulate myogenic differentiation in a context-dependent manner, possibly because of the specific partners of the JAK–STAT complex[29,30].

To investigate the specific role of Stat3 in satellite cells, we assessed its activation during muscle regeneration. We performed skeletal muscle injury by intramuscular injection of notexin (NTX), a snake venom toxin that induces myofiber damage and a strong regenerative response[31]. We observed transient Stat3 phosphorylation on Tyr705 in Pax7^{+} satellite cells while they were actively engaged in tissue repair (**Supplementary Fig. 1**). After isolation and culture, satellite cells are activated rapidly and transition to the progenitor stage. We detected Stat3 phosphorylation in freshly isolated satellite cells from 2-month-old C57BL/6 mice after 4 d in culture. This phosphorylation was positively correlated with expression of *Myod1*, a basic helix-loop-helix (bHLH) myogenic regulatory factor that is characteristic of committed progenitors (**Fig. 1a**), suggesting that Stat3 activation could be involved in cell fate decisions.

To test whether a functional interaction exists between Stat3 and Myod1, we infected satellite cells isolated from 2-month-old C57BL/6 mice with a lentivirus expressing shRNA against Stat3 (shStat3) or a control shRNA (shControl). Infection with shStat3 efficiently down-regulated Stat3 and impaired the expression of Myod1 and myogenin (**Fig. 1b**,**c**, **Supplementary Fig. 2a** and **Supplementary Table 1**). Notably, shStat3 infection promoted the expansion of Pax7^{+} satellite cells (**Fig. 1d** and **Supplementary Fig. 2b**). We observed no difference in apoptosis, as shown by TUNEL assay (**Supplementary Fig. 2c**). Consistent with previous reports associating Il-6–mediated Stat3 phosphorylation with satellite cell function[23,32], we demonstrated that Il-6 stimulation is associated with higher mRNA levels of both

[1]Graduate School of Biomedical Sciences, Sanford-Burnham Medical Research Institute, La Jolla, California, USA. [2]Development, Aging and Regeneration Program (DARe), Sanford-Burnham Medical Research Institute, La Jolla, California, USA. [3]Life Sciences Solutions, Thermo Fisher Scientific, Carlsbad, California, USA. [4]Epigenetics and Regenerative Medicine, Istituto di Ricovero e Cura a Carattere Scientifico (IRCCS) Fondazione Santa Lucia, Rome, Italy. [5]Institute of Translational Pharmacology, National Research Council of Italy, Rome, Italy. [6]These authors equally contributed to this work. Correspondence should be addressed to A.S. (asacco@sanfordburnham.org).

Received 4 February; accepted 10 July; published online 7 September 2014; doi:10.1038/nm.3656

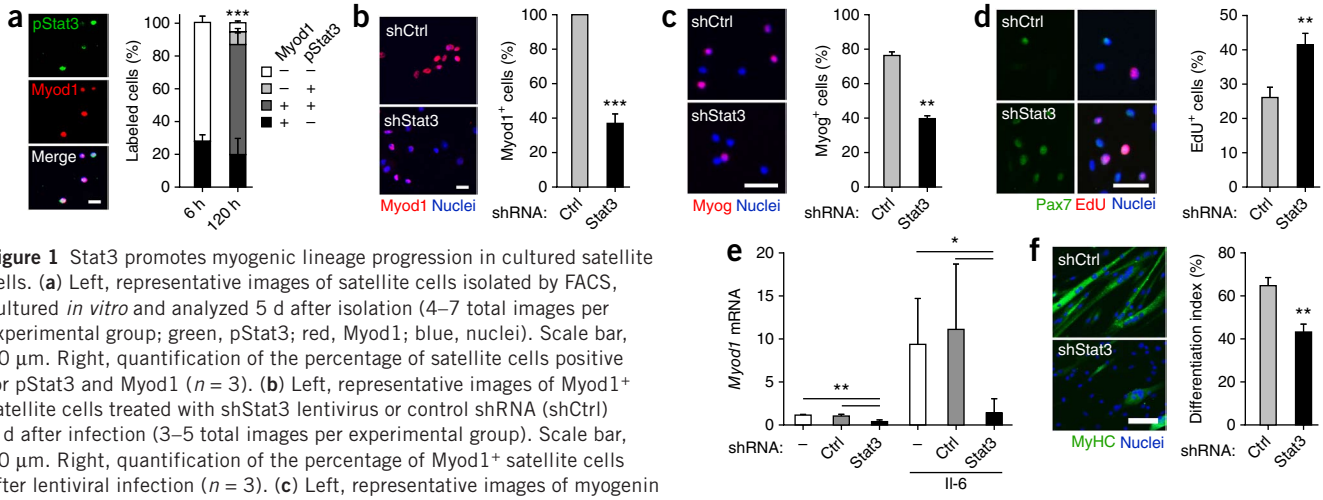

Figure 1 Stat3 promotes myogenic lineage progression in cultured satellite cells. (**a**) Left, representative images of satellite cells isolated by FACS, cultured *in vitro* and analyzed 5 d after isolation (4–7 total images per experimental group; green, pStat3; red, Myod1; blue, nuclei). Scale bar, 50 µm. Right, quantification of the percentage of satellite cells positive for pStat3 and Myod1 ($n = 3$). (**b**) Left, representative images of Myod1$^+$ satellite cells treated with shStat3 lentivirus or control shRNA (shCtrl) 4 d after infection (3–5 total images per experimental group). Scale bar, 50 µm. Right, quantification of the percentage of Myod1$^+$ satellite cells after lentiviral infection ($n = 3$). (**c**) Left, representative images of myogenin (Myog)$^+$ satellite cells infected with shStat3 or shCtrl and cultured in growth medium for 72 h (3 images total per experimental group). Scale bar, 50 µm. Right, quantification of the percentage of Myog$^+$ cells after lentiviral infection ($n = 3$). (**d**) Left, representative images of Pax7$^+$EdU$^+$ satellite cells treated with shStat3 or shCtrl lentiviruses 4 d after infection (3–5 images total per experimental group). Scale bar, 50 µm. Right, quantification of the percentage of EdU$^+$ satellite cell after lentiviral infection ($n = 5$). (**e**) Quantification of *Myod1* mRNA levels in satellite cells infected with shStat3 or shCtrl lentivirus and maintained in culture in growth medium in either the absence or presence of 100 ng ml^{-1} IL-6 for 96 h ($n = 4$). (**f**) Left, representative images of differentiated myosin heavy chain (MyHC)$^+$ myotubes (green, MyHC; blue, nuclei) in satellite cells that were infected with shStat3 or shCtrl lentivirus and analyzed 72 h after terminal differentiation was induced (3–5 total images per experimental group). Scale bar, 50 µm. Right, quantification of differentiation index in satellite cells after shStat3 treatment ($n = 3$). All data are represented as the average ± s.e.m. Student's *t* test was used for all statistical analyses (***$P < 0.001$, **$P < 0.01$, *$P < 0.05$) except in **e**, where one-way analysis of variance (ANOVA) with Tukey's post test was used.

Stat3 and *Myod1* when compared to untreated samples. Stat3 mediated this effect, as IL-6–dependent *Myod1* upregulation was impaired after infection with the shStat3 lentivirus (**Fig. 1e** and **Supplementary Fig. 2d**). In agreement with previous studies[29,30], Stat3 loss of function impaired terminal myogenic differentiation of satellite cells, as shown by a lower differentiation index compared to shControl (**Fig. 1f**). These findings indicate that IL-6–mediated advancement of satellite cells to the progenitor stage is dependent on Stat3, whose expression is required for proper myogenic differentiation.

To further examine the regulatory role of Stat3 on *Myod1* transcription, we performed bioinformatics analyses and identified a putative STAT3 consensus sequence in the regulatory element of the *Myod1* locus 590 bp upstream of the transcription start site[33,34]. To investigate the contribution of Stat3 to *Myod1* activation, we cloned the *Myod1* regulatory region containing the putative Stat3 binding site upstream of the firefly luciferase (Fluc) reporter gene (**Supplementary Fig. 3a**). We transfected the reporter plasmid into 293 cells in the presence or absence of shStat3 or a *Myod1* overexpression vector. Although Myod1 could promote Fluc reporter activity through sustained positive feedback[35], shStat3 resulted in markedly lower activation compared to shControl, indicating its essential role in *Myod1* expression.

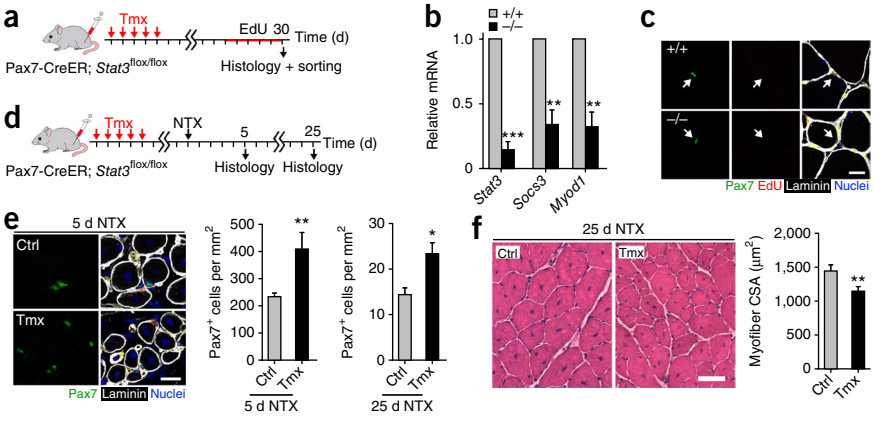

Figure 2 *Stat3* gene deletion enhances satellite cell expansion after skeletal muscle injury. (**a**) Schematic representation of Tmx treatment in male and female 2-month-old Pax7-CreER; *Stat3*$^{flox/flox}$ and Pax7-CreER; *Stat3*$^{+/+}$ mice. EdU was administered daily for 5 d before harvesting. (**b**) *Stat3*, *Myod1* and *Socs3* mRNA levels in satellite cells isolated from the uninjured skeletal muscle of Tmx-treated Pax7-CreER; *Stat3*$^{flox/flox}$ and Pax7-CreER; *Stat3*$^{+/+}$ mice after culture in growth medium for 96 h ($n = 3$). (**c**) Representative images of uninjured skeletal muscle of Tmx-treated Pax7-CreER; *Stat3*$^{flox/flox}$ and Pax7-CreER; *Stat3*$^{+/+}$ mice (10–15 total images per experimental group; arrow, Pax7$^+$ satellite cell; green, Pax7; red, EdU; white, laminin; blue, nuclei). Scale bar, 20 µm. (**d**) Schematic representation of Tmx or vehicle treatment and skeletal muscle injury in male and female 2-month-old Pax7-CreER; *Stat3*$^{flox/flox}$ mice. (**e**) Left, representative images of Pax7$^+$ satellite cells within the muscles of Tmx- or vehicle (Ctrl)-treated Pax7-CreER; *Stat3*$^{flox/flox}$ mice 5 d after injury (6–18 total images per experimental group; green, Pax7; white, laminin; blue, nuclei). Scale bar, 50 µm. Right, quantification of Pax7$^+$ satellite cell numbers in regenerating muscles at 5 and 25 d after injury ($n = 3$). (**f**) Left, representative images of H&E staining of the muscles of Tmx- or vehicle (Ctrl)-treated Pax7-CreER; *Stat3*$^{flox/flox}$ mice 25 d after injury (5 total images per experimental group). Scale bar, 50 µm. Right, quantification of average myofiber cross-sectional area 25 d after injury ($n = 3$). All data are represented as the average ± s.e.m. Student's *t* test was used for all statistical analyses (***$P < 0.001$, **$P < 0.01$, *$P < 0.05$).

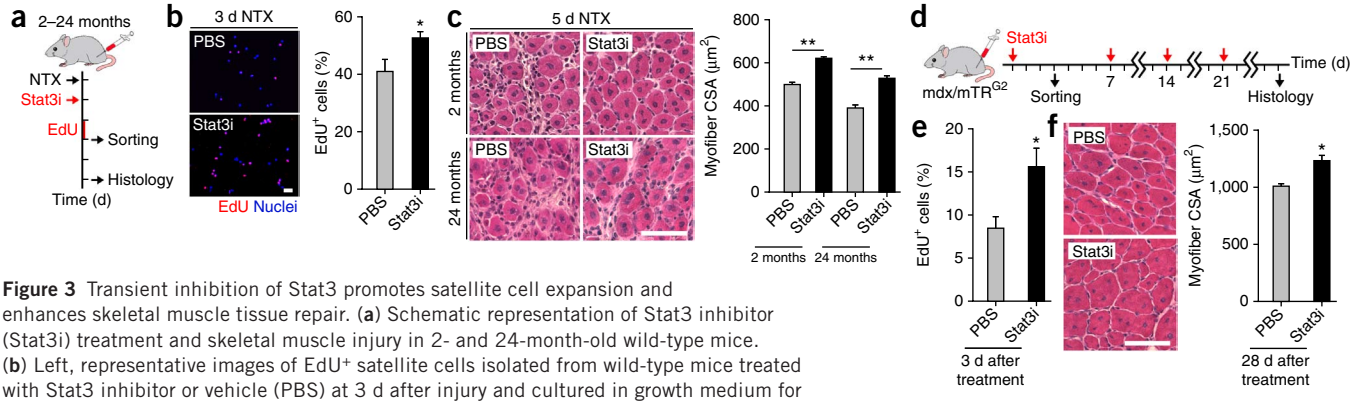

Figure 3 Transient inhibition of Stat3 promotes satellite cell expansion and enhances skeletal muscle tissue repair. (**a**) Schematic representation of Stat3 inhibitor (Stat3i) treatment and skeletal muscle injury in 2- and 24-month-old wild-type mice. (**b**) Left, representative images of EdU$^+$ satellite cells isolated from wild-type mice treated with Stat3 inhibitor or vehicle (PBS) at 3 d after injury and cultured in growth medium for 2 h (5 total images per experimental group). Scale bar, 50 μm. Right, quantification of the percentage of EdU$^+$ satellite cells ($n = 3$). (**c**) Left, representative images of H&E staining in regenerating muscles of 2- and 24-month-old mice treated with the Stat3 inhibitor or vehicle control at 5 d after injury (5 total images per experimental group). Scale bar, 50 μm. Right, quantification of average myofiber cross-sectional area (CSA) in regenerating muscles of 2- and 24-month-old mice 5 d after injury ($n = 3$). (**d**) Schematic representation of Stat3 inhibitor treatment in skeletal muscles of dystrophic 2-month-old mdx/mTR^{G2} mice. (**e**) Quantification of the percentage of EdU$^+$ satellite cells isolated from mice treated with the Stat3 inhibitor or vehicle control ($n = 3$). (**f**) Left, representative images of H&E staining of muscles of mdx/mTR^{G2} mice treated with the Stat3 inhibitor or vehicle control at 28 d (10 total images per experimental group). Scale bar, 50 μm. Right, quantification of average myofiber cross-sectional area at 28 d ($n = 3$). All data are represented as the average ± s.e.m. Student's *t* test was used for all statistical analyses (**$P < 0.01$, *$P < 0.05$).

Chromatin immunoprecipitation sequencing (ChIP-seq) experiments in C2C12 myoblasts previously showed an enrichment in histone H3 Lys 27 (H3K27) acetylation at this Stat3 consensus sequence that typically defines activated enhancers[36,37]. Indeed, we detected H3K27 acetylation at the putative Stat3 binding site of *Myod1* and its downstream target *Socs3* by ChIP in primary myoblasts (**Supplementary Fig. 3b**). Inactive enhancers (i.e., IgH) and the promoters of repressed genes (i.e., *Oct4*, also called *Pou5f1*, and *Pdx1*) did not show detectable H3K27 acetylation. These findings are consistent with Stat3 loss-of-function experiments in myoblasts demonstrating a reduction in both Stat3 and Myod1 expression at the mRNA and protein levels (**Supplementary Fig. 3c**,**d**), further demonstrating a role for Stat3 in promoting myogenic lineage progression.

To evaluate the requirement of Stat3 for satellite cell function *in vivo*, we conditionally ablated Stat3 in satellite cells using 2-month-old Pax7-CreER; *Stat3*$^{flox/flox}$ mice[38,39] (**Fig. 2a**). After tamoxifen (Tmx) treatment in these mice, Cre-mediated recombination results in permanent *Stat3* gene deletion under control of the Pax7-CreER driver. We confirmed that Tmx treatment efficiently ablated *Stat3* in satellite cells, lowered *Myod1* and *Socs3* mRNA levels and resulted in higher satellite cell proliferation *in vitro* (**Fig. 2b** and **Supplementary Fig. 4b**,**c**). *Stat3* gene deletion was not sufficient to break satellite cell quiescence in healthy muscles, as we detected no changes in the percentage of 5-ethynyl-2′-deoxyuridine (EdU)$^+$ satellite cells, suggesting a role for Stat3 signaling only after satellite cell activation (**Fig. 2c**). Still, the loss of *Stat3* expression altered the behavior of physiologically activated satellite cells as demonstrated by a higher total number of Pax7$^+$ satellite cells after 30 d (**Supplementary Fig. 4d**). When we performed *Stat3* gene deletion in 3-month-old mice, there was no detectable difference in the number of Pax7$^+$ satellite cells when compared to Pax7-CreER; *Stat3*$^{+/+}$ mice, indicating an age-dependent effect of *Stat3* gene deletion. We observed no difference in myofiber size (**Supplementary Fig. 4e**). Genetic loss of *Stat3* was associated with a greater number of Pax7$^+$ satellite cells at both 5 and 25 d after NTX injury (**Fig. 2d**,**e**). However, regeneration was impaired, as indicated by smaller myofiber size 25 d after injury compared to vehicle-treated mice (**Fig. 2f**), emphasizing the requirement of Stat3 for proper myogenic differentiation.

We reasoned that the use of Stat3 inhibitors would enable the transient expansion of satellite cells without preventing their contribution to regenerating myofibers. Indeed, presentation of a Stat3 inhibitor to cultured satellite cells from 2-month-old C57BL/6 mice resulted in the previously observed downregulation of *Myod1* and *Socs3* mRNA and increase in proliferation at 96 h (**Supplementary Fig. 5a**,**b**). When we

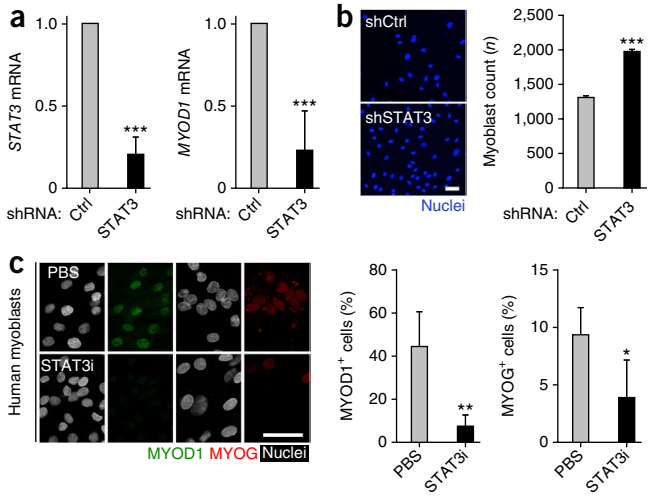

Figure 4 The effects of STAT3 manipulation are conserved in human myoblasts. (**a**) *STAT3* and *MYOD1* mRNA levels in human myoblasts infected with shSTAT3 lentivirus or shControl (shCtrl) at 96 h after infection ($n = 4$). (**b**) Left, representative images of human myoblasts infected with shSTAT3 lentivirus or shCtrl and cultured for 96 h (16 total images per experimental group; blue, nuclei). Scale bar, 50 μm. Right, quantification of total human myoblast numbers 96 h after infection ($n = 3$). (**c**) Left, representative images of human myoblasts treated with the STAT3 inhibitor or vehicle control for 72 h (10–15 total images per experimental group; green, MYOD1; red, myogenin (MYOG); white, nuclei). Scale bar, 50 μm. Right, quantification of the percentage of MYOD1$^+$ and MYOG$^+$ human myoblasts after STAT3 inhibitor treatment ($n = 4$). All data are represented as the average ± s.e.m. Student's *t* test was used for all statistical analyses (***$P < 0.001$, **$P < 0.01$, *$P < 0.05$).

injected the Stat3 inhibitor into regenerating muscles of 2-month-old C57BL/6 mice, we detected a higher percentage of EdU$^+$ proliferating satellite cells 3 d after NTX injury compared to vehicle-treated mice (**Fig. 3a**,**b**). This effect was transient, as we observed no detectable difference in the number of Pax7$^+$ satellite cells 5 d after injury (**Supplementary Fig. 5c**,**d**). Administration of the Stat3 inhibitor accelerated tissue repair, as we observed larger regenerating myofibers at 5 d after injury in treated muscles. This effect was not maintained at 25 d (**Fig. 3c** and **Supplementary Fig. 6a–d**). The Stat3 inhibitor had no direct effect on mature myofiber size when presented to uninjured muscles (**Supplementary Fig. 5e**,**f**).

To examine Stat3 as a potential therapeutic target, we analyzed two distinct contexts of impaired muscle regeneration: aged and dystrophic muscles. Notably, Stat3 inhibitor treatment accelerated tissue repair in the regenerating muscles of aged (24-month-old) mice (**Fig. 3c** and **Supplementary Fig. 6b–d**). To evaluate the effects of the Stat3 inhibitor in dystrophic conditions, we used a severe model of muscular dystrophy, the mdx/mTR^{G2} mouse[6]. This double mutant lacks both dystrophin and the RNA component of telomerase, combining chronic muscle degeneration with telomere dysfunction and shortening to more closely recapitulate the human disease. Stat3 inhibitor administration to these mice promoted the short-term expansion of satellite cells, as shown by EdU incorporation 3 d after treatment (**Fig. 3d**,**e**). Dystrophic muscle undergoes continuous cycles of regeneration and degeneration; thus, we hypothesized that repeated administration of the Stat3 inhibitor would support reoccurring satellite cell expansion while still allowing for their contribution to myofiber repair. To test this hypothesis, we delivered the Stat3 inhibitor once per week to the mdx/mTR^{G2} mice for 28 d. We detected larger regenerating myofibers in the muscles of inhibitor-treated mice when compared to vehicle-treated mice, indicating an overall improvement in muscle repair (**Fig. 3f** and **Supplementary Fig. 7**). Together these findings indicate that intermittent Stat3 inhibition could be a promising approach to improve tissue repair in diseased conditions.

In addition, we found that the impact of STAT3 inhibition on proliferation and *MYOD1* transcription was conserved in human myoblasts derived from healthy patients 12–14 years of age. Infection of human myoblasts with the shSTAT3 lentivirus downregulated *MYOD1* expression and promoted proliferation compared to shControl (**Fig. 4a**,**b**). STAT3 inhibitor treatment of the cells also downregulated the expression of phosphorylated STAT3 (pSTAT3), MYOD1 and myogenin (**Fig. 4c** and **Supplementary Fig. 8a**). Apoptosis was not affected in these experimental conditions (**Supplementary Fig. 8b**). Human myoblasts treated previously with the STAT3 inhibitor were able to efficiently give rise to multinucleated myotubes after treatment was lifted, validating the preservation of differentiation potential after transient STAT3 inhibition across species (**Supplementary Fig. 8c**).

Using both molecular and genetic approaches, we demonstrated that STAT3 signaling promotes myogenic lineage progression, thereby inhibiting the expansion of the satellite cells during skeletal muscle repair. The choice between self-renewal and differentiation is critical to simultaneously ensure satellite cell pool maintenance while also generating differentiated progeny. Fine tuning the temporal interpretation of microenvironmental cues in satellite cells may be able to delay progression along the myogenic lineage. Our results indicate that the timing of STAT3 activation in satellite cells signifies a molecular switch between these two states. We speculate that prolonged STAT3 activation resulting from chronic degenerative stimuli might favor pro-differentiation pathways and ultimately lead to a progressive, functional exhaustion of the satellite cell pool.

We show that the use of a Stat3 inhibitor promoted the expansion of satellite cells in the initial phases of regeneration, accelerating tissue repair. Cyclic administration of the Stat3 inhibitor during chronic regenerative conditions was able to promote muscle repair, possibly by augmenting repeated rounds of satellite cell expansion. These findings are consistent with previous studies demonstrating that inhibition of tumor necrosis factor (TNF)-p38 (also called MAPK14) signaling, which promotes myogenic commitment, resulted in satellite cell expansion[40–42]. Conservation of the phenotypic effects of STAT3 in human myoblasts validates STAT3 as a promising therapeutic target to ameliorate muscle wasting.

METHODS

Methods and any associated references are available in the online version of the paper.

Note: Any Supplementary Information and Source Data files are available in the online version of the paper.

ACKNOWLEDGMENTS

We thank A. Cortez, J. Morales and B. Charbono for technical support. We thank the following Stanford-Burnham Medical Research Institute Core Facilities for technical support: Vivarium, Flow Cytometry, Viral Core and Cell Imaging. We thank S. Akira (Osaka University) and S. Schenk (University of California, San Diego) for providing the *Stat3*$^{flox/flox}$ mice, C. Keller (Oregon Health and Science University) and H. Makarenkova (The Scripps Research Institute) for providing the Pax7-CreER mice and H.M. Blau (Stanford University) for providing the mdx/mTR^{G2} mice. We thank M. Karin (University of California, San Diego) for providing the shSTAT3 construct. We thank EuroBioBank and the Telethon Network of Genetic Biobanks (GTB12001F) for providing the human biological samples. This work was supported by US National Institutes of Health (NIH) grants P30 AR061303 and R03 AR063328 and the Sanford-Burnham Center to A.S., California Institute for Regenerative Medicine (CIRM) Training grant TG2 001162 to T.A., an Italian Foreign Ministry (MAE) grant to L.L. and NIH grants R01AR056712, R01AR052779 and P30 AR061303 to P.L.P.

AUTHOR CONTRIBUTIONS

A.S., M.T.T. and T.A. designed the experiments. T.A. performed the *in vitro* lentivirus and STAT3 inhibitor experiments. T.A., D.S. and M.T.T. performed experiments in the Pax7-CreER; *Stat3*$^{flox/flox}$ mice. M.T.T. performed experiments with the STAT3 inhibitor in young, aged and dystrophic mice. B.M. performed the ChIP analysis. S.G. performed the bioinformatics analysis. L.L. performed the studies on human myoblasts. All authors discussed and interpreted data. A.S., P.L.P., M.T.T., T.A. and D.S. drafted and revised the manuscript.

COMPETING FINANCIAL INTERESTS

The authors declare no competing financial interests.

1. Seale, P. *et al.* Pax7 is required for the specification of myogenic satellite cells. *Cell* **102**, 777–786 (2000).
2. Collins, C.A. *et al.* Stem cell function, self-renewal, and behavioral heterogeneity of cells from the adult muscle satellite cell niche. *Cell* **122**, 289–301 (2005).
3. Montarras, D. *et al.* Direct isolation of satellite cells for skeletal muscle regeneration. *Science* **309**, 2064–2067 (2005).
4. Sacco, A., Doyonnas, R., Kraft, P., Vitorovic, S. & Blau, H.M. Self-renewal and expansion of single transplanted muscle stem cells. *Nature* **456**, 502–506 (2008).
5. Cerletti, M. *et al.* Highly efficient, functional engraftment of skeletal muscle stem cells in dystrophic muscles. *Cell* **134**, 37–47 (2008).
6. Sacco, A. *et al.* Short telomeres and stem cell exhaustion model Duchenne muscular dystrophy in mdx/mTR mice. *Cell* **143**, 1059–1071 (2010).
7. Lepper, C., Partridge, T.A. & Fan, C.M. An absolute requirement for Pax7-positive satellite cells in acute injury-induced skeletal muscle regeneration. *Development* **138**, 3639–3646 (2011).
8. Sambasivan, R. *et al.* Pax7-expressing satellite cells are indispensable for adult skeletal muscle regeneration. *Development* **138**, 3647–3656 (2011).
9. Murphy, M.M., Lawson, J.A., Mathew, S.J., Hutcheson, D.A. & Kardon, G. Satellite cells, connective tissue fibroblasts and their interactions are crucial for muscle regeneration. *Development* **138**, 3625–3637 (2011).

10. Chakkalakal, J.V., Jones, K.M., Basson, M.A. & Brack, A.S. The aged niche disrupts muscle stem cell quiescence. *Nature* **490**, 355–360 (2012).
11. Sousa-Victor, P. *et al.* Geriatric muscle stem cells switch reversible quiescence into senescence. *Nature* **506**, 316–321 (2014).
12. Tidball, J.G. Inflammatory processes in muscle injury and repair. *Am. J. Physiol. Regul. Integr. Comp. Physiol.* **288**, R345–R353 (2005).
13. Fearon, K.C., Glass, D.J. & Guttridge, D.C. Cancer cachexia: mediators, signaling, and metabolic pathways. *Cell Metab.* **16**, 153–166 (2012).
14. Strassmann, G., Fong, M., Kenney, J.S. & Jacob, C.O. Evidence for the involvement of interleukin 6 in experimental cancer cachexia. *J. Clin. Invest.* **89**, 1681–1684 (1992).
15. Bonetto, A. *et al.* STAT3 activation in skeletal muscle links muscle wasting and the acute phase response in cancer cachexia. *PLoS ONE* **6**, e22538 (2011).
16. Muñoz-Cánoves, P., Scheele, C., Pedersen, B.K. & Serrano, A.L. Interleukin-6 myokine signaling in skeletal muscle: a double-edged sword? *FEBS J.* **280**, 4131–4148 (2013).
17. Zhang, L. *et al.* Stat3 activation links a C/EBPδ to myostatin pathway to stimulate loss of muscle mass. *Cell Metab.* **18**, 368–379 (2013).
18. Kiger, A.A., Jones, D.L., Schulz, C., Rogers, M.B. & Fuller, M.T. Stem cell self-renewal specified by JAK-STAT activation in response to a support cell cue. *Science* **294**, 2542–2545 (2001).
19. Tulina, N. & Matunis, E. Control of stem cell self-renewal in *Drosophila* spermatogenesis by JAK-STAT signaling. *Science* **294**, 2546–2549 (2001).
20. Oh, I.H. & Eaves, C.J. Overexpression of a dominant negative form of STAT3 selectively impairs hematopoietic stem cell activity. *Oncogene* **21**, 4778–4787 (2002).
21. Doles, J., Storer, M., Cozzuto, L., Roma, G. & Keyes, W.M. Age-associated inflammation inhibits epidermal stem cell function. *Genes Dev.* **26**, 2144–2153 (2012).
22. Haddad, F., Zaldivar, F., Cooper, D.M. & Adams, G.R. IL-6–induced skeletal muscle atrophy. *J. Appl. Physiol. (1985)* **98**, 911–917 (2005).
23. Serrano, A.L., Baeza-Raja, B., Perdiguero, E., Jardi, M. & Munoz-Canoves, P. Interleukin-6 is an essential regulator of satellite cell–mediated skeletal muscle hypertrophy. *Cell Metab.* **7**, 33–44 (2008).
24. Zeidler, M.P., Bach, E.A. & Perrimon, N. The roles of the *Drosophila* JAK/STAT pathway. *Oncogene* **19**, 2598–2606 (2000).
25. Gorissen, M., de Vrieze, E., Flik, G. & Huising, M.O. STAT genes display differential evolutionary rates that correlate with their roles in the endocrine and immune system. *J. Endocrinol.* **209**, 175–184 (2011).
26. Darnell, J.E. Jr., Kerr, I.M. & Stark, G.R. Jak-STAT pathways and transcriptional activation in response to IFNs and other extracellular signaling proteins. *Science* **264**, 1415–1421 (1994).
27. Zhong, Z., Wen, Z. & Darnell, J.E. Jr. Stat3: a STAT family member activated by tyrosine phosphorylation in response to epidermal growth factor and interleukin-6. *Science* **264**, 95–98 (1994).
28. Takeda, K. *et al.* Targeted disruption of the mouse Stat3 gene leads to early embryonic lethality. *Proc. Natl. Acad. Sci. USA* **94**, 3801–3804 (1997).
29. Sun, L. *et al.* JAK1-STAT1-STAT3, a key pathway promoting proliferation and preventing premature differentiation of myoblasts. *J. Cell Biol.* **179**, 129–138 (2007).
30. Wang, K., Wang, C., Xiao, F., Wang, H. & Wu, Z. JAK2/STAT2/STAT3 are required for myogenic differentiation. *J. Biol. Chem.* **283**, 34029–34036 (2008).
31. Harris, J.B. & MacDonell, C.A. Phospholipase A2 activity of notexin and its role in muscle damage. *Toxicon.* **19**, 419–430 (1981).
32. Megeney, L.A., Perry, R.L., LeCouter, J.E. & Rudnicki, M.A. bFGF and LIF signaling activates STAT3 in proliferating myoblasts. *Dev. Genet.* **19**, 139–145 (1996).
33. Goldhamer, D.J., Faerman, A., Shani, M. & Emerson, C.P. Jr. Regulatory elements that control the lineage-specific expression of myoD. *Science* **256**, 538–542 (1992).
34. Tapscott, S.J., Lassar, A.B. & Weintraub, H. A novel myoblast enhancer element mediates MyoD transcription. *Mol. Cell. Biol.* **12**, 4994–5003 (1992).
35. Penn, B.H., Bergstrom, D.A., Dilworth, F.J., Bengal, E. & Tapscott, S.J.A. MyoD-generated feed-forward circuit temporally patterns gene expression during skeletal muscle differentiation. *Genes Dev.* **18**, 2348–2353 (2004).
36. Asp, P. *et al.* Genome-wide remodeling of the epigenetic landscape during myogenic differentiation. *Proc. Natl. Acad. Sci. USA* **108**, E149–E158 (2011).
37. Heintzman, N.D. *et al.* Histone modifications at human enhancers reflect global cell-type–specific gene expression. *Nature* **459**, 108–112 (2009).
38. Takeda, K. *et al.* Stat3 activation is responsible for IL-6–dependent T cell proliferation through preventing apoptosis: generation and characterization of T cell–specific Stat3-deficient mice. *J. Immunol.* **161**, 4652–4660 (1998).
39. Nishijo, K. *et al.* Biomarker system for studying muscle, stem cells, and cancer *in vivo*. *FASEB J.* **23**, 2681–2690 (2009).
40. Palacios, D. *et al.* TNF/p38α/polycomb signaling to Pax7 locus in satellite cells links inflammation to the epigenetic control of muscle regeneration. *Cell Stem Cell* **7**, 455–469 (2010).
41. Bernet, J.D. *et al.* p38 MAPK signaling underlies a cell-autonomous loss of stem cell self-renewal in skeletal muscle of aged mice. *Nat. Med.* **20**, 265–271 (2014).
42. Cosgrove, B.D. *et al.* Rejuvenation of the muscle stem cell population restores strength to injured aged muscles. *Nat. Med.* **20**, 255–264 (2014).

ONLINE METHODS

Animals. All protocols were approved by the Sanford-Burnham Medical Research Institute Animal Care and Use Committee. Pax7-CreER (a kind gift from C. Keller[39]) and *Stat3*$^{flox/flox}$ (a kind gift from S. Akira[38]) mice were used to generate Pax7-CreER; *Stat3*$^{flox/flox}$ mice. The colony was maintained in a C57BL/6 background. Young (2–3 months of age) C57BL/6 male mice were purchased from Jackson Laboratories. Aged C57BL/6 male mice (24 months of age) were obtained from the National Institute of Aging. mdx/mTR^{G2} mice (2 months of age) were kindly donated by H.M. Blau[6].

Satellite cell isolation. Satellite cells were isolated as described previously with minor revisions[4]. Tibialis anterior, gastrocnemius and quadriceps muscles of mice (mouse model specified in the text) were subjected to enzymatic dissociation (0.2% collagenase and 0.02 units ml^{-1} dispase; Sigma) for 45 min, after which non-muscle tissue was gently removed and the muscle was minced under a dissection microscope, followed by another 45-min incubation. The cell suspension was filtered through a 70-μm nylon filter and incubated with the following biotinylated rat antibodies: CD45 (clone 30–F11), CD11b (cat #553309), CD31 (cat #5011513) and Sca1 (clone E13–161.7) (all BD Bioscience and 1:150 dilution). Streptavidin beads (Miltenyi Biotech, 1:10 dilution) were then added to the cells together with the following antibodies: integrin-α_7–phycoerythrin (PE) (cat #R2F2, Ablab, 1:100 dilution) and CD34–Alexa 647 (clone RAM34, eBioscience, 1:50 dilution), after which magnetic depletion of biotin-positive cells was performed. The (CD45$^-$CD11b$^-$CD31$^-$Sca1$^-$) CD34$^+$integrin-α_7^+ population was then fractionated by flow cytometry (BD FACSAria), followed by a purity check.

Cell lines. We obtained C2C12 cells (crl-1772) and 293 cells (crl-1573) from ATCC. We obtained human myoblasts from Lonza Group Ltd, EuroBioBank and the Telethon Network of Genetic Biobanks (GTB12001F), which had been isolated from the quadriceps of four healthy patients 12–14 years of age. Informed consent to use their biological samples for diagnosis and research was obtained from the patients in accordance with protocols approved by the Institutional Review Board of the C. Besta Neurological Institute. We isolated myoblasts by enzymatic digestion of human skeletal muscle tissue. Cells were not recently authenticated or tested for mycoplasma contamination.

Human cell culture. Human myoblasts were cultured in either growth medium (DMEM, 20% FBS, GlutaMAX, 10 ng ml^{-1} insulin, 24 ng ml^{-1} basic fibroblast growth factor (bFGF), 10 ng ml^{-1} epidermal growth factor (EGF) and penicillin and streptomycin) or differentiation medium (DMEM, 5% horse serum and 100 ng ml^{-1} insulin).

Immunofluorescence. Muscle tissues (mouse model specified in the text) were prepared for histology as described previously[4]. Cells and muscle sections were fixed with 1.5% paraformaldehyde (PFA) and permeabilized in 0.3% Triton X-100 followed by 100% methanol for 5 min at −20 °C for pSTAT3 staining. Cells were then blocked in 20% goat serum and 0.3% Triton X-100 for 1 h. For Pax7 staining, antigen retrieval was performed, and sections were post fixed with 1.5% PFA. Incubation with the primary antibodies was performed overnight at 4 °C. The antibodies used were as follows: rabbit anti-pSTAT3 (Tyr705, D3A7, Cell Signaling, 1:50 dilution), mouse anti-Pax7 (Developmental Studies Hybridoma Bank (DSHB), 1:100 dilution), rat anti-laminin (clone A5, Millipore, 1:150 dilution), mouse anti-Myod1 (cat#554130, BD Bioscience, 1:100 dilution), rabbit anti-Myod1 (cat#sc760, Santa Cruz, 1:100 dilution), mouse anti-myogenin (cat #556358, BD Biosciences, 1:100 dilution), mouse anti–myosin heavy chain (cat #MF20, DHSB, 1:100 dilution) and Alexa-conjugated secondary antibodies (Invitrogen, 1:200 dilution). Nuclei were counterstained with Hoechst 33258 (Invitrogen). Cell proliferation was measured by EdU incorporation (Life Technologies). Cell death was measured by TUNEL assay (Roche). Images of cell cultures were acquired using an inverted epifluorescent microscope (Nikon TE300), 10× objective lens, charge-coupled device (CCD) SPOT RT camera and SPOT imaging software (Diagnostic Instruments). Images of muscle transverse sections were acquired using the Nikon TE300 or the LSM170 laser-scanning confocal microscope, Plan-Apochromat 20×/0.8 objective lens and ZEN 2011 imaging software (Zeiss). All images were composed and edited, and modifications were applied to the whole image using Photoshop CS6 (Adobe).

Quantification of satellite cell numbers and myofiber size in histological sections. We analyzed 10-μm-thick histological sections of skeletal muscle tissues (mouse model specified in the text). For regenerating muscles, only the regenerating areas were assessed. We defined regenerating areas as areas containing centrally nucleated myofibers. Analysis was performed using ImageJ software.

Tmx treatment and skeletal muscle injury. We used Pax7-CreER; *Stat3*$^{flox/flox}$ male and female mice between the ages of 6 and 12 weeks for Tmx injections. Tmx (3 mg) suspended in corn oil was injected intraperitoneally (i.p.) each day for 5 d. After 7 d from the last injection, tibialis anterior muscles were injured with 10 μl of (10 μg ml^{-1}) notexin intramuscularly. 20 μg per kg body weight EdU was administered i.p. Tissues were harvested after 3, 5, 25 and 30 d for FACS or histological analysis. We used corn oil or Pax7-CreER; *Stat3*$^{+/+}$ mice as a control for i.p. injections, as indicated.

STAT3 inhibitor treatment. For *in vitro* studies, 50 μM STAT3 inhibitor (Calbiochem) was supplemented in growth medium. For *in vivo* studies in wild-type mice, 50 μg STAT3 inhibitor was injected intramuscularly (i.m.) 24 h after NTX injury. In mdx/mTR^{G2} mice, 50 μg STAT3 inhibitor was injected i.m. to the tibialis anterior muscle every 7 d. 20 μg per kg body weight EdU was administered i.p. 24 h before harvest (every 12 h). Tissues were harvested after 3, 5, 25 and 28 d for FACS or histological analysis.

Lentiviral infection. High-titer lentiviral production of all lentivectors was performed at the Viral Vectors Facility at the Sanford-Burnham Medical Research Institute (La Jolla, CA). 96-well plates were coated with laminin (20 μg ml^{-1}) for 45 min at 37 °C. Afterwards, plates were coated with retronectin (15 μg ml^{-1}) for 2 h at room temperature. 2% BSA was used to wash for 30 min, followed by PBS washing twice at room temperature. 2,000 satellite cells from 2-month-old C57BL/6 male mice were infected with shLuciferase (labeled as shControl), shStat3 and PGK-Myod1 (45% DMEM low glucose, 40% F10, 15% FBS and 2.5 ng ml^{-1} bFGF). Cell plates were centrifuged at 300*g* for 1 min and left overnight at 37 °C and 5% CO_2. The medium was changed the next day and was replaced with fresh medium every 48 h; EdU was presented to cells (20 μM) for 4 h before harvest after 4 d in culture.

RNA analysis by quantitative PCR. RNA was extracted from cells (source specified in the text) using Qiagen RNeasy mini-kits and micro-kits following the manufacturer's protocol. Total RNA was quantified with a Nanodrop 8000 spectrophotometer (Thermo Scientific, Wilmington). First-strand cDNA was synthesized from total RNA using the Transcriptor First Strand cDNA Synthesis kit (Roche) following the manufacturer's protocols. The generated cDNA was used as a template in real-time PCR reactions with Lightcycler 480 SYBR Green 1 master mix (Roche) and was run on a Roche LC480 machine using three-step amplification and melt curve analysis. Quantitative real-time PCR reactions consisted of 2× SYBR Green Supermix (Roche), 0.25 mmol l^{-1} forward and reverse primers (**Supplementary Table 1**) and 10 ng cDNA. Relative gene expression was normalized by dividing the specific expression value by the glyceraldehyde 3-phosphate dehydrogenase (Gapdh) expression value and calculated using the $2^{-\delta\Delta CT}$ method.

Western blotting. Western blotting was performed as previously described with minor modifications[15]. Total protein extract was obtained by homogenizing primary myoblasts in RIPA buffer (150 mM NaCl, 1.0% NP-40, 0.5% sodium deoxycholate, 0.1% SDS and 50 mM Tris, pH 8.0) added with a protease inhibitor cocktail (Roche, Indianapolis, IN, USA) and incubated at 4 °C for 30 min, centrifuging for 1 min every 10 min. Cell debris was removed by centrifugation, and the supernatant was collected and stored at −80 °C. Protein concentration was determined using the Pierce BSA protein assay kit. Total protein extracts (30 μg) were then electrophoresed in gradient SDS gels and 1× MES SDS running buffer (Invitrogen). Gels were transferred to polyvinylidene difluoride

doi:10.1038/nm.3656

membranes. Membranes were blocked with 1× Tris-buffered saline (TBS) and 0.1% Tween-20 (TBST) with 5% (w/v) BSA at room temperature for 1 h, followed by an overnight incubation with diluted antibody in blocking buffer at 4 °C with gentle shaking. After washing with TBST, the membrane was incubated at room temperature for 1 h with a goat polyclonal anti-rabbit IgG secondary antibody conjugated to horseradish peroxidase (HRP) (Santa Cruz, 1:10,000 dilution). Membranes were visualized with enhanced chemiluminescence (Pierce Supersignal Pico or ECL 2), followed by exposure to film. The antibodies used were as follows: rabbit anti–total Stat3 (79D7, Cell Signaling, 1:1,000 dilution), rabbit anti-pStat3 (D3A7, Cell Signaling, 1:1,000 dilution), rabbit anti-Gapdh (D16H11, Cell Signaling, 1:10,000) and mouse anti-Myod1 (cat#554130, BD Pharmingen, 1:1,000 dilution).

ChIP. Primary myoblasts were crosslinked with 1% formaldehyde in TBS for 15 min at room temperature. Crosslinked cells were washed with cold TBS containing 1 mM PMSF, harvested and lysed in a ChIP lysis buffer containing 50 mM Tris-HCl, pH 8.0, 150 mM NaCl, 5 mM EDTA, pH 8.0, 0.5% SDS, 0.5% NP-40, 1 mM PMSF and a protease and phosphatase inhibitor cocktail (Roche). Cell lysates were diluted five times with the ChIP lysis buffer lacking SDS to the final concentration of 0.1% SDS. Chromatin was sheared to an average DNA fragment length of 500 bp using a Misonix3000 sonicator. Samples were centrifuged and the protein concentration of soluble chromatin was determined by bicinchoninic acid (BCA) assay (Pierce). 110 μg chromatin was used for immunoprecipitation with 5 μg of anti-H3K27Ac antibody (39133, Active Motif) and 5 μg of an unspecific normal rabbit IgG as a control (sc-2027, Santa Cruz). After 2 h incubation of the chromatin with the antibodies at 4 °C, the immunocomplexes were captured with protein A magnetic beads (Life Technologies) for a further 4 h at 4 °C. Protein A–bound immunocomplexes were washed four times with buffer containing 50 mM Tris-HCl, pH 8.0, 150 mM NaCl, 5 mM EDTA, pH 8.0, 0.1% SDS, 1% NP-40, 0.5% sodium deoxycholate, 1 mM PMSF and a protease and phosphatase inhibitor cocktail (Roche), followed by one wash with a buffer containing 250 mM LiCl, 100 mM NaCl, 5 mM EDTA, pH 8.0, 1% NP-40, 1% sodium deoxycholate and a protease inhibitor cocktail (Roche) and a subsequent final two washes with Tris + EDTA (TE) buffer. Immunocomplexes were eluted from the beads for 15 min at 65 °C with buffer containing 50 mM Tris-Cl, pH 8.0, 1 mM EDTA, pH 8.0, and 1% SDS. Crosslinking was reversed by incubation of the ChIP-isolated immunocomplexes and the input chromatin samples at 65 °C overnight in the presence of 200 mM NaCl. After 0.2 mg ml^{-1} proteinase K treatment of samples, DNA from the immunoprecipitated samples as well as DNA from the 2% input were purified by phenol and chloroform extraction and ethanol precipitation. 1/50 of the purified DNA was analyzed by real-time quantitative PCR using SYBR Green PCR Master Mix (Applied Biosystems). The ChIP signal was evaluated by calculating the amount of immunoprecipitated DNA relative to the input DNA (percentage of input).

Luciferase assay. The 1.2-kb promoter region of Myod1 (from the pBabePuro-Myod vector) was subcloned into a pGL 4.22 Luciferase reporter vector (Promega). Luciferase and *Renilla* activity were measured using the Dual Luciferase Reporter Assay System (Promega) following the manufacturer's protocol.

Statistical analyses. Data are presented as the mean ± s.e.m. Comparisons between groups used Student's *t* test assuming two-tailed distributions, with an α level of 0.05. When comparing more than two sets, one-way ANOVA with Tukey's post test was performed using GraphPad Prism 6 for Macintosh (http://www.graphpad.com). All experiments requiring the use of animals, directly or as a source of cells, were subjected to randomization based on litter. Investigators were not blinded to group allocation or outcome assessment. Sample size was predetermined based on the variability observed in preliminary and similar experiments. No samples or animals were excluded from this study.